Robust entanglement with three-dimenstional nonreciprocal photonic topological insulators

S. Ali Hassani Gangaraj, George W. Hanson, Mauro Antezza

▶ **To cite this version:**

S. Ali Hassani Gangaraj, George W. Hanson, Mauro Antezza. Robust entanglement with three-dimenstional nonreciprocal photonic topological insulators. Physical Review A : Atomic, molecular, and optical physics [1990-2015], 2017, 95, pp.063807. 10.1103/PhysRevA.95.063807 . hal-01533723

HAL Id: hal-01533723
https://hal.science/hal-01533723

Submitted on 13 Oct 2020

HAL is a multi-disciplinary open access archive for the deposit and dissemination of scientific research documents, whether they are published or not. The documents may come from teaching and research institutions in France or abroad, or from public or private research centers.

L'archive ouverte pluridisciplinaire **HAL**, est destinée au dépôt et à la diffusion de documents scientifiques de niveau recherche, publiés ou non, émanant des établissements d'enseignement et de recherche français ou étrangers, des laboratoires publics ou privés.

Robust entanglement with three-dimensional nonreciprocal photonic topological insulators

S. Ali Hassani Gangaraj,[1,*] George W. Hanson,[1,†] and Mauro Antezza[2,3,‡]

[1]*Department of Electrical Engineering, University of Wisconsin-Milwaukee, 3200 North Cramer Street, Milwaukee, Wisconsin 53211, USA*

[2]*Laboratoire Charles Coulomb (L2C), UMR 5221, Centre National de la Recherche Scientifique, Universit de Montpellier, F-34095 Montpellier, France*

[3]*Institut Universitaire de France, 1 rue Descartes, F-75231 Paris Cedex 05, France*

(Received 29 January 2017; published 6 June 2017)

We investigate spontaneous and pumped entanglement of two-level systems in the vicinity of a photonic topological insulator interface, which supports a nonreciprocal (unidirectional), scattering-immune, and topologically protected surface-plasmon polariton in the band gap of the bulk material. To this end, we derive a master equation for qubit interactions in a general three-dimensional, nonreciprocal, inhomogeneous, and lossy environment. The environment is represented exactly, via the photonic Green's function. The resulting entanglement is shown to be extremely robust to defects occurring in the material system, such that strong entanglement is maintained even if the interface exhibits electrically large and geometrically sharp discontinuities. Alternatively, depending on the initial excitation state, using a nonreciprocal environment allows two qubits to remain unentangled even for very close spacing. The topological nature of the material is manifest in the insensitivity of the entanglement to variations in the material parameters that preserve the gap Chern number. Our formulation and results should be useful for both fundamental investigations of quantum dynamics in nonreciprocal environments and technological applications related to entanglement in two-level systems.

DOI: 10.1103/PhysRevA.95.063807

I. INTRODUCTION

Entanglement as a quantum resource is important for a range of emerging applications, including quantum computing [1] and quantum cryptography [2]. A main obstacle to the development of entanglement-based systems is decoherence associated with the unavoidable coupling between a quantum system and the degrees of freedom of the surrounding environment [3]. However, reservoir engineering methods have changed the idea of trying to minimize coupling to the environment to one of modifying the properties of the environment in order to achieve a desired state. These methods include using dissipative dynamics [4–9], recently extended to systems out of thermal equilibrium [10–14], as well as, e.g., exploiting the effect of measurements and feedback to achieve a desired final state [15,16].

Another emerging resource for reservoir engineering is the use of nonreciprocal environments [17]. In particular, there has been considerable investigation of quantum spin networks in chiral waveguides [18–24]. The previous work on spin dynamics in quantum chiral environments has focused on one-dimensional (1D) waveguide models. Here, we investigate two-level (spin) qubit interactions mediated by unidirectional surface-plasmon polaritions (SPPs) at the interface of a photonic topological insulator (PTI) and a topological-trivial material.

PTIs represent a broad class of materials that are attracting wide interest for both fundamental and applied reasons [25–28]. Perhaps their most celebrated aspect is their ability to support SPPs that are unidirectional, propagate in the bulk band gap, and are topologically protected from backscattering at discontinuities [29–36]. PTIs can be broadly divided into two classes: (i) those with broken time-reversal symmetry, which are photonic analogs of quantum Hall insulators [photonic quantum Hall effect (PQHE)], and (ii) those that are time-reversal invariant but have broken inversion symmetry, which are photonic analogs of electronic topological insulators or quantum spin Hall insulators [photonic quantum spin Hall Effect (PQSHE)]. Although as a specific example we consider PTIs of the PQHE type, the formulation presented here is general.

In this paper, we develop a master equation (ME) for three-dimensional (3D), nonreciprocal, inhomogeneous, and lossy environments, based on the macroscopic canonical quantization scheme described in [37–39], extended to nonreciprocal media [40]. In Sec. II A we present the master equation (derived in Appendix A), and in Sec. II B we provide the equations for concurrence as a measure of entanglement. In Sec. III we consider the topological aspect of concurrence for a PQHE-type PTI system consisting of a plasma continuum. Then, qubit entanglement dynamics are examined for several waveguiding systems. We focus on the aspects unique to the topological and nonreciprocal environment, such as the preservation of entanglement in the presence of large defects. Three appendices present a derivation of the master equation and discussion of various approximations, a comparison with previous 1D chiral MEs and discussion of the 1D, two-dimensional (2D), and 3D Green's functions, and a derivation of the unidirectional concurrence.

II. THEORETICAL MODEL

In this section, we first present a general ME valid for both reciprocal and nonreciprocal, inhomogeneous, and lossy environments. This form is valid for 3D, 2D, and 1D systems since it is expressed in terms of the electromagnetic Green's function. Then, we present concurrence expressions for the

*ali.gangaraj@gmail.com
†george@uwm.edu
‡mauro.antezza@umontpellier.fr

 ©2017 American Physical Society

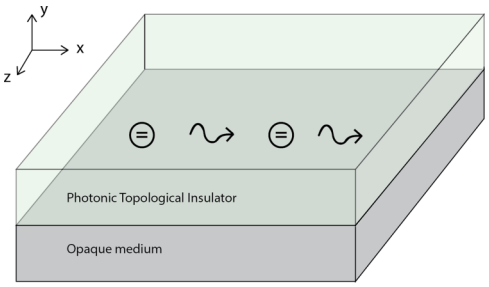

FIG. 1. Two qubits at the interface of a PTI and topologically trivial medium. The resulting unidirectional SPP provides a strongly nonreciprocal environment for qubit entanglement.

unidirectional case. The physical system we will consider is that of two qubits at the interface of a PTI and another (eventually topologically trivial) medium, as depicted in Fig. 1, although the development is completely general.

A. Master equation for general 3D nonreciprocal environments

We consider qubits with transition frequency ω_0 interacting through a general nonreciprocal environment. For a derivation in the reciprocal case, see [41].

The classical electric field satisfies

$$\left[\nabla\times\mu^{-1}(\mathbf{r},\omega)\nabla\times-\frac{\omega^2}{c^2}\varepsilon(\mathbf{r},\omega)\right]\mathbf{E}(\mathbf{r},\omega)=i\omega\mu_0\mathbf{j}_s(\mathbf{r},\omega), \tag{1}$$

where c is the vacuum speed of light, $\mu(\mathbf{r},\omega)$ and $\boldsymbol{\varepsilon}(\mathbf{r},\omega)$ are the material permeability and permittivity, and $\mathbf{j}_s(\mathbf{r},\omega)$ is the noise current. In this paper, we suppose that the medium is nonmagnetic, $\mu(\mathbf{r},\omega)=\mathbf{I}$, where $\mathbf{I}$ is the unit dyad, but that the permittivity is a tensorial quantity. By defining the noise current in terms of polarization as $\mathbf{j}_s=-i\omega\mathbf{P}_s$, which is associated with material absorption by the fluctuation-dissipation theorem, the electric-field Green's tensor is the solution of

$$\left[\nabla\times\nabla\times-\frac{\omega^2}{c^2}\varepsilon(\mathbf{r},\omega)\right]\mathbf{G}(\mathbf{r},\mathbf{r}',\omega)=\mathbf{I}\delta(\mathbf{r},\mathbf{r}'), \tag{2}$$

and the electric field is $\mathbf{E}(\mathbf{r},\omega)=(\omega^2/c^2\varepsilon_0)\int_V d\mathbf{r}'\mathbf{G}(\mathbf{r},\mathbf{r}',\omega)\cdot\mathbf{P}_s(\mathbf{r}',\omega)$. Following the standard macroscopic canonical quantization [37–39], the noise polarization can be expressed in terms of the bosonic field annihilation operator as [40]

$$\hat{\mathbf{P}}_s(\mathbf{r},\omega)=-i\sqrt{\frac{\hbar\varepsilon_0}{\pi}}\mathbf{T}(\mathbf{r},\omega)\cdot\hat{\mathbf{f}}(\mathbf{r},\omega), \tag{3}$$

where

$$\mathbf{T}(\mathbf{r},\omega)\cdot\mathbf{T}^\dagger(\mathbf{r},\omega)=\frac{1}{2i}[\boldsymbol{\varepsilon}(\mathbf{r},\omega)-\boldsymbol{\varepsilon}^\dagger(\mathbf{r},\omega)], \tag{4}$$

and, for the special case of a symmetric permittivity tensor (e.g., a reciprocal medium), $\mathbf{T}(\mathbf{r},\omega)=\sqrt{\mathrm{Im}\boldsymbol{\varepsilon}(\mathbf{r},\omega)}$. The bosonic field operators $\hat{\mathbf{f}}(\mathbf{r},\omega)$ obey the commutation relations $[\hat{\mathrm{f}}_j(\mathbf{r},\omega),\hat{\mathrm{f}}^\dagger_{j'}(\mathbf{r}',\omega')]=\delta_{jj'}\delta(\mathbf{r}-\mathbf{r}')\delta(\omega-\omega')$ and $[\hat{\mathrm{f}}_j(\mathbf{r},\omega),\hat{\mathrm{f}}_{j'}(\mathbf{r}',\omega')]=0$. The noise polarization operator generates the electric-field operator

$$\hat{\mathbf{E}}(\mathbf{r},\omega)=i\sqrt{\frac{\hbar}{\pi\varepsilon_0}}\frac{\omega^2}{c^2}\int d\mathbf{r}'\mathbf{G}(\mathbf{r},\mathbf{r}',\omega)\cdot\mathbf{T}(\mathbf{r},\omega)\cdot\hat{\mathbf{f}}(\mathbf{r}',\omega), \tag{5}$$

where $\mathbf{G}(\mathbf{r},\mathbf{r}',\omega)$ is the classical electric-field Green's tensor. Using this formulation, we arrive at the master equation (see Appendix A for details)

$$\partial_t\rho_s(t)=-\frac{i}{\hbar}[\mathrm{H}_s+\mathrm{V}^{AF},\rho_s(t)]+\mathcal{L}\rho(t), \tag{6}$$

where

$$\begin{aligned}\mathcal{L}\rho_s(t)=&\sum_i\frac{\Gamma_{ii}(\omega_0)}{2}(2\sigma_i\rho_s(t)\sigma_i^\dagger-\sigma_i^\dagger\sigma_i\rho_s(t)-\rho_s(t)\sigma_i^\dagger\sigma_i)\\&+\sum_{i,j}^{i\neq j}\frac{\Gamma_{ij}(\omega_0)}{2}([\sigma_j\rho_s(t),\sigma_i^\dagger]+[\sigma_i,\rho_s(t)\sigma_j^\dagger])\\&+\sum_{i,j}^{i\neq j}g_{ij}(\omega_0)([\sigma_j\rho_s(t),-i\sigma_i^\dagger]+[i\sigma_i,\rho_s(t)\sigma_j^\dagger]).\end{aligned} \tag{7}$$

Equation (7) is applicable to both reciprocal and nonreciprocal environments and an arbitrary number of qubits. In Eq. (7), $\mathcal{L}$ is the Lindblad superoperator for the general nonreciprocal medium, involving the dissipative decay rate, $\Gamma_{ij}(\omega_0)$, and the coherent coupling terms, $g_{ij}(\omega_0)$, in terms of the electromagnetic Green's dyadic evaluated at the qubit transition frequency ω_0:

$$\begin{aligned}\Gamma_{ij}(\omega_0)&=\frac{2\omega_0^2}{\varepsilon_0\hbar c^2}\sum_{\alpha,\beta=x,y,z}d_{\alpha i}\mathrm{Im}[\mathrm{G}_{\alpha\beta}(\mathbf{r}_i,\mathbf{r}_j,\omega_0)]d_{\beta j},\\g_{ij}(\omega_0)&=\frac{\omega_0^2}{\varepsilon_0\hbar c^2}\sum_{\alpha,\beta=x,y,z}d_{\alpha i}\mathrm{Re}[\mathrm{G}_{\alpha\beta}(\mathbf{r}_i,\mathbf{r}_j,\omega_0)]d_{\beta j}.\end{aligned} \tag{8}$$

The Hamiltonian of the decoupled qubits is

$$\mathrm{H}_s=\sum_i\hbar\Delta\omega_i\sigma_i^\dagger\sigma_i, \tag{9}$$

where $\Delta\omega_i=\omega_0-\omega_l-\delta_i$, with $\delta_i=g_{ii}$ being the Lamb shift and ω_l the laser frequency of an external source. The Lamb shift for optical emitters is in general on the order of a few GHz, therefore the effect of the Lamb shift for optical frequencies is small ($\omega_i\sim10^{15}$ Hz, $\delta_i\sim10^9$ Hz), and can be ignored, or assumed to be accounted for in the definition of the transition frequency ω_0. In Eq. (6), the term

$$\begin{aligned}\mathrm{V}^{AF}=&-\hbar(\Omega_1e^{-i\Delta_lt}\sigma_1^\dagger+\Omega_1^*e^{i\Delta_lt}\sigma_1)\\&-\hbar(\Omega_2e^{-i\Delta_lt}\sigma_2^\dagger+\Omega_2^*e^{i\Delta_lt}\sigma_2)\end{aligned} \tag{10}$$

represents the external coherent drive applied to each qubit at laser frequency ω_l. Due to its large amplitude we treat the drive field as a c number where $\Omega_i=\mathbf{d}_i\cdot\mathbf{E}_0^i/\hbar$ is a Rabi frequency and $\Delta_l=\omega_0-\omega_l$ is the detuning parameter.

For the reciprocal case where $\Gamma_{ij}=\Gamma_{ji}$ and $g_{ij}=g_{ji}$ it can be shown that Eq. (7) is the well-known reciprocal (bidirectional) master equation [42,43]. In the reciprocal case, some terms associated with $g_{ij}=g_{ji}$ cancel each other out and are eliminated from the dissipative term. For example,

$\sigma_i \rho_s(t) \sigma_j^\dagger, i \neq j$, appears in the nonreciprocal case but is absent in the reciprocal case.

For a system of two qubits, Eq. (7) can be written in the simple form

$$\begin{aligned}\mathcal{L}\rho_s(t) = &\sum_{j=1,2} \frac{\Gamma_{jj}}{2}(2\sigma_j \rho_s \sigma_j^\dagger - \rho_s \sigma_j^\dagger \sigma_j - \sigma_j^\dagger \sigma_j \rho_s) \\ &+ \left(\frac{\Gamma_{21}}{2} + i g_{21}\right)(\sigma_2 \rho_s \sigma_1^\dagger - \rho_s \sigma_1^\dagger \sigma_2) \\ &+ \left(\frac{\Gamma_{21}}{2} - i g_{21}\right)(\sigma_1 \rho_s \sigma_2^\dagger - \sigma_2^\dagger \sigma_1 \rho_s) \\ &+ \left(\frac{\Gamma_{12}}{2} + i g_{12}\right)(\sigma_1 \rho_s \sigma_2^\dagger - \rho_s \sigma_2^\dagger \sigma_1) \\ &+ \left(\frac{\Gamma_{12}}{2} - i g_{12}\right)(\sigma_2 \rho_s \sigma_1^\dagger - \sigma_1^\dagger \sigma_2 \rho_s). \end{aligned} \tag{11}$$

A comparison with previous 1D chiral ME formulations is provided in Appendix B.

B. Transient entanglement: Unidirectional SPP-assisted qubit communication

In this paper, all numerical results are computed using the master equation (6) with the general 3D Lindblad superoperator Eq. (7), where the Green's tensor for complicated environments is obtained numerically. However, as shown in Appendix C, if the system of qubits is communicating through a strongly nonreciprocal environment, e.g., $\mathbf{G}(\mathbf{r}_1, \mathbf{r}_2) = 0$ ($\Gamma_{12} = g_{12} = 0$) and $\mathbf{G}(\mathbf{r}_2, \mathbf{r}_1) \neq 0$, then the concurrence (as a measure of entanglement [44]) is

$$\begin{aligned}\mathcal{C}(t) &= 2\sqrt{\frac{\Gamma_{21}^2}{4} + g_{21}^2} t e^{-\Gamma_{11} t} \\ &= 2\frac{\omega_0^2 d_y^2}{\hbar \varepsilon_0 c^2} |\mathbf{G}_{yy}(\mathbf{r}_2, \mathbf{r}_1, \omega_0)| t e^{-\Gamma_{11} t}, \end{aligned} \tag{12}$$

where it has been assumed that the qubits are both polarized along the y axis. This is the general unidirectional result. Concurrence reaches its maximum value at $t = 1/\Gamma_{11}$, such that $\mathcal{C}_{\max} = 2\sqrt{\tilde{\Gamma}_{12}^2/4 + \tilde{g}_{21}^2}/e$, where $\tilde{\Gamma}_{21}$ and $\tilde{g}_{21}$ are rates normalized by Γ_{11}.

Although the Hamiltonian in nonreciprocal systems is non-Hermitian, it can be seen (Appendix C) that the density matrix is Hermitian, probability conservation holds ($\mathrm{Tr}(\rho) = 1$), and that diagonal elements of the density operator can be interpreted as population densities, as for Hermitian Hamiltonians.

For two identical qubits interacting through a reciprocal medium,

$$\begin{aligned}\mathcal{C}_{\mathrm{recip}}(t) = \Big\{ &\tfrac{1}{4}[e^{-(\Gamma_{11}+\Gamma_{12})t} - e^{-(\Gamma_{11}-\Gamma_{12})t}]^2 \\ &+ e^{-2\Gamma_{11} t} \sin^2(2 g_{12} t) \Big\}^{1/2}. \end{aligned} \tag{13}$$

One of the main differences between the concurrence in the reciprocal case Eq. (13), and in the unidirectional case Eq. (12), is the presence of the sinusoidal term in Eq. (13). When g_{12} is strong enough, this sinusoidal term causes oscillations in the transient concurrence related to photons being recycled between the two qubits, with a period that corresponds to the round trip time of the coupled qubits through the reciprocal medium (Rabi oscillations). For the unidirectional case Eq. (12) Rabi oscillations cannot occur.

It was shown in [43] that for qubits coupled to an infinite reciprocal waveguide system, the positions of Γ_{ij} maxima or minima correspond to positions of g_{ij} minima or maxima (for finite waveguides, see [45]). Thus, in general, coherent and dissipative regimes become dominant at different separations between emitters. It was further shown in [43] that for an infinite reciprocal plasmonic waveguide the best entanglement was obtained when Γ_{ij} was large and g_{ij} was small (forming the dissipative regime), which forces a restriction on the positioning of the qubits in the reciprocal case. However, in the unidirectional case the qubit positioning is unimportant, as detailed in [18], and the qubits can be anywhere in the coherent or dissipative regimes, which is a practical advantage of these unidirectional systems. In three dimensions it is also true that being in the coherent or dissipative regime makes no difference for a unidirectional system, as evidenced by Eq. (12), where it is seen that large concurrence arises merely from the magnitude of the Green's function being large.

III. NUMERICAL RESULTS

A unidirectional SPP can be provided by the interface between a PTI and a topologically trivial material. When operated in a common band gap of the two materials (or if the trivial medium is opaque), the SPP is unidirectional, topologically protected from backscattering, and diffraction immune, providing an ideal implementation of a strongly nonreciprocal system for qubit interactions. Although here we implement a PTI as a PQHE using a continuum plasma [34–36], many other implementations of PTIs are possible, of both PQHE and PQSHE types, and qualitatively would behave in a similar manner.

A. Continuum photonic topological insulator realization of a nonreciprocal SPP environment

We assume a magnetized plasma having the permittivity tensor

$$\underline{\varepsilon} = \begin{bmatrix} \varepsilon_{11} & i\varepsilon_{12} & 0 \\ -i\varepsilon_{12} & \varepsilon_{11} & 0 \\ 0 & 0 & \varepsilon_{33} \end{bmatrix} \tag{14}$$

where

$$\begin{aligned}\varepsilon_{11} &= 1 + i\frac{\omega_p^2}{\omega}\left(\frac{\nu - i\omega}{(\nu - i\omega)^2 + \omega_c^2}\right), \\ \varepsilon_{12} &= \frac{\omega_p^2 \omega_c}{\omega\left[(\nu - i\omega)^2 + \omega_c^2\right]}, \quad \varepsilon_{33} = 1 + i\frac{\omega_p^2}{\omega(\nu - i\omega)}, \end{aligned} \tag{15}$$

and where $\omega_c = (q_e/m_e)B_z$ is the cyclotron frequency (B_z is the applied bias field), $\omega_p^2 = N_e q_e^2/\varepsilon_0 m_e$ is the squared plasma frequency (N_e is the free-electron density and q_e and m_e are the electron charge and mass, respectively), and ν

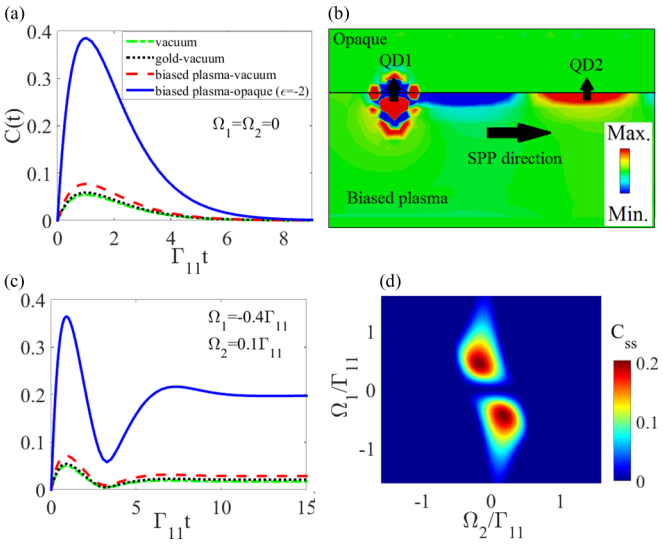

FIG. 2. (a) Transient concurrence for two interacting qubits in different environments: (1) vacuum, (2) at the interface of a gold half space ($\varepsilon = -91.6 - 3i$) and vacuum, (3) at the interface of a magnetized plasma ($\omega_p/\omega_0 = 0.95, \omega_c/\omega_0 = 0.21$) and vacuum, and (4) at the interface of the magnetized plasma and an opaque medium (nonbiased plasma with $\omega_p/\omega_0 = \sqrt{3}$, such that $\varepsilon = -2$). (b) One way SPP at the interface of the biased plasma and the opaque medium at $\omega_0/2\pi = 200$ THz. (c) Driven concurrence of two qubits in the same environments as in panel (a). (d) Steady-state concurrence vs pumping intensities for the case of the biased plasma and opaque medium interface. The qubit separation is 2.4 μm (1.6λ_0) and they are placed in the plasma region, very close to the interface at $y = \lambda_0/60$. For other plots in this paper we assume the same qubit location with respect to the interface.

is the collision frequency. Initially, we set $\nu = 0$ to focus on the effect of unidirectionality, but later the effect of loss is considered. The magnetized plasma is able to support a bulk TE mode with dispersion $k_{\rm TE}^2 = \varepsilon_{33}(\omega/c)^2$ and a bulk TM mode with dispersion $k_{\rm TM}^2 = \varepsilon_{\rm eff}(\omega/c)^2$, where $\varepsilon_{\rm eff} = (\varepsilon_{11}^2 - \varepsilon_{12}^2)/\varepsilon_{11}$ [33]. Both bulk modes are reciprocal. The Chern number of the bulk TE mode is trivial, and so TE modes are not considered further in this paper. The Chern numbers of the bulk TM modes are nonzero, and at the interface of the magnetized plasma and a topologically trivial (simple) medium the gap Chern number is $C_{\rm gap} = 1$ [34,35], indicating the presence of one nonreciprocal, backscattering-immune TM SPP that crosses the band gap (band structure is shown later, in Fig. 3).

B. Entanglement evaluation in different environments

We first consider the behavior of the concurrence for qubits in several different environments, and establish that the best entanglement occurs for a PTI–opaque-medium interface. Figure 2(a) shows a comparison of concurrence between four different cases of two qubits interacting (1) through vacuum, (2) at the interface of a gold half space and vacuum, (3) at the interface of a magnetized plasma and vacuum, and (4) at the interface of a magnetized plasma and an opaque medium. Here and in the following, the Green's function is calculated numerically [46], and the qubits are considered to be placed very close to the interface, at $y = \lambda_0/60$ in the plasma region. However, we numerically found that all plots and conclusions remain unchanged when the qubits are at a distance at least a height $< \lambda_0/30$ in the plasma region.

The system of qubits was initially prepared in state $|4\rangle = |e_1\rangle \otimes |g_2\rangle$, such that the left qubit is initially in the excited state while the right qubit is in the ground state.

From Fig. 2(a), it is clear that the biased-plasma–opaque medium interface is far superior to the other cases. The poor performance of the gold-vacuum interface is somewhat surprising, since a strong SPP can be excited and the separation is chosen to be in the dissipative regime, which is a best-case scenario for the reciprocal case. Making the gold lossless does not significantly improve the concurrence (results not shown). The problem is primarily due to the lack of lateral confinement of the SPP, since in [43,45], where various waveguide geometries are used to confine the mode, concurrence values are obtained much better than vacuum values. The unidirectional case has much higher C even for the flat interface, since energy is focused in one direction. Furthermore, for the biased-plasma case, one bulk region is opaque and the other has a band gap, and so no radiation goes into either bulk medium, whereas for a gold-vacuum interface energy can flow into the vacuum. Thus, in the following, we focus on the magnetized-plasma–opaque-medium geometry.

Figure 2(b) shows the excited unidirectional SPP at the interface of the magnetized plasma and the opaque medium, demonstrating the unidirectional nature of the SPP, and Fig. 2(c) shows the case of pumped concurrence, where the qubit depopulation is compensated by applying an external laser source in resonance with the atomic transition frequency. The pump intensity must be chosen carefully, as illustrated in Fig. 2(d), which shows the steady-state concurrence for a wide range of laser intensities (a laser pump can be applied to the qubits via, e.g., a fiber penetrating into the material). It can be seen that the laser intensity cannot be too large, otherwise the qubits will interact mostly with the laser. Ideally, the pump should be strong enough to keep the system interacting, but weak enough for the qubit interaction to dominate the dynamics. It is clear from Fig. 2(d) that unequal pumping leads to larger steady-state concurrence.

C. Topological aspect of entanglement

In this section we briefly show the topological aspect of entanglement in a PTI system. Figure 3 shows the reciprocal bulk bands (solid blue) for the biased plasma, and the unidirectional gap-crossing SPP (dashed red) dispersion for a biased-plasma–opaque-medium interface, for different values of bias. For $\omega_c > 0$ the gap Chern number is -1 [34,35], and there is a positive-traveling SPP ($v_g = d\omega/dk > 0$), topologically protected against backscattering. At $\omega_c = 0$ the gap closes, the material becomes topologically trivial (gap Chern number is zero), and there exists a reciprocal SPP. For $\omega_c < 0$ the gaps reopens, the gap Chern number is 1, and there is a negative-traveling SPP ($v_g < 0$), topologically protected against backscattering.

Figure 4 shows the concurrence when the left dot has an initial excitation (state $|4\rangle = |e_1, g_2\rangle$). The concurrence is rather insensitive to the bias as long as the topology does

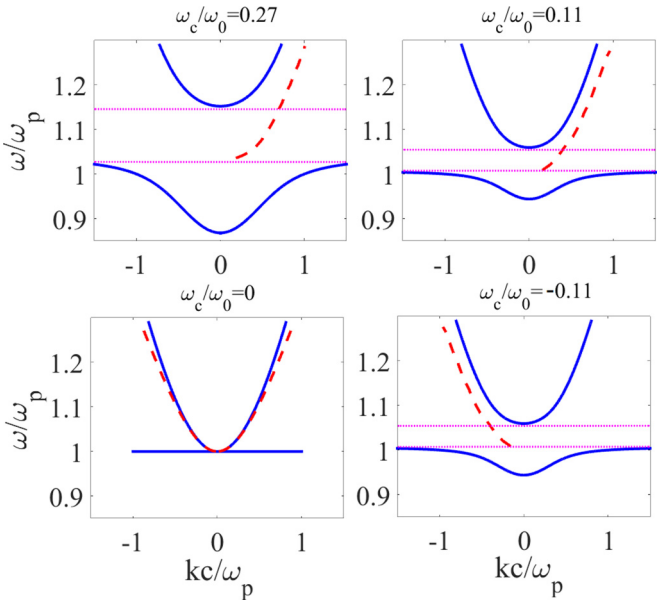

FIG. 3. Reciprocal bulk bands (solid blue) for the biased plasma ($\omega_p/\omega_0 = 0.95$), and the unidirectional gap-crossing SPP (dashed red) dispersion for a biased-plasma–opaque-medium ($\varepsilon = -2$) interface, for different values of bias at $\omega_0/2\pi = 200$ THz. In the nonreciprocal cases the gap Chern number is 1.

not change; however, when the gap closes and reopens the concurrence vanishes.

D. Preserving entanglement in the presence of large defects

Perhaps the most important aspect of using PTIs for entanglement is the possibility of robust SPPs, topologically immune to backscattering (and immune to diffraction if operated in the bulk band gap) in the presence of any arbitrary large obstacle or defect. To examine this, we compare two cases: (1) the interface between an opaque medium and a biased plasma and (2) the interface between the same opaque medium and an unbiased plasma.

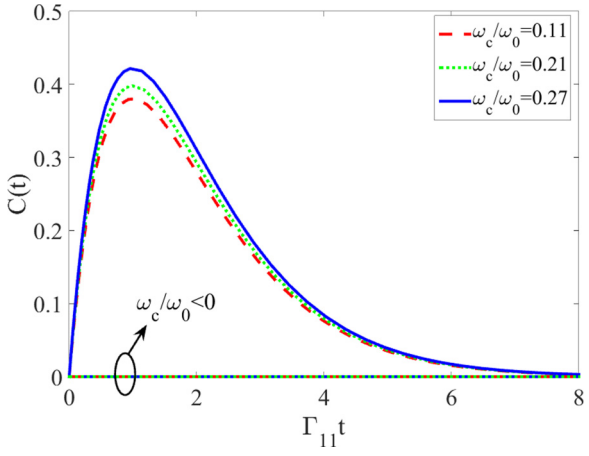

FIG. 4. Concurrence mediated by a unidirectional SPP at the interface of biased plasma ($\omega_p/\omega_0 = 0.95$) and an opaque medium ($\varepsilon = -2$) when the left dot has an initial excitation (state $|4\rangle = |e_1, g_2\rangle$). For $\omega_c < 0$, the same three absolute values are considered as for positive bias, i.e., $\omega_c/\omega_0 = -|0.27|, -|0.21|$, and $-|0.11|$. The qubit separation is 2.4 μm ($1.6\lambda_0$) and $\omega_0/2\pi = 200$ THz.

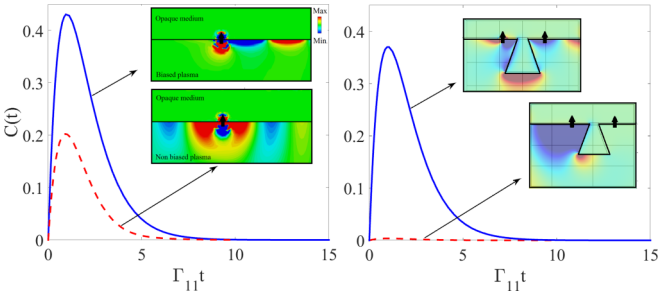

FIG. 5. Left panel: Transient concurrence of two qubits interacting through a flat interface made of an opaque medium ($\varepsilon = -2$) and both an unbiased plasma ($\omega_p/\omega_0 = 0.95$, $\omega_c/\omega_0 = 0$) and a biased plasma ($\omega_p/\omega_0 = 0.95$, $\omega_c/\omega_0 = 0.21$). Inset: Electric field E_y excited by a vertical electric dipole. Right panel: Same thing for the case of a defected interface, where the defect contour length is of the order of a free-space wavelength. The system of qubits is initially prepared in the state $|4\rangle = |e_1, g_2\rangle$. The qubit separation is 1.7 μm ($1.13\lambda_0$) and $\omega_0/2\pi = 200$ THz.

In the nonreciprocal case, this unidirectional and scattering-immune SPP provides the ability to preserve the entangled state of two qubits in plasmonic systems even in the presence of very nonideal interfaces. Figure 5 shows the transient concurrence for the cases of biased or unbiased plasmas with flat and defected interfaces. Although for the flat interface the biased plasma provides better concurrence than the reciprocal (unbiased) case, this could be perhaps altered by adjustment of the two material half-space properties. However, the point is that in the presence of a defect, as shown in the right panel, the reciprocal SPP suffers from a strong reflection at the defect, as expected, whereas the nonreciprocal SPP (biased plasma) detours around the defect, leading to the same concurrence as without the defect.

E. Finite-width waveguide

The previous results were for an infinitely wide interface. In this section we examine the effect of lateral confinement of the SPP [35]. Figure 6(a) shows the finite-width waveguide geometry. In order to efficiently confine the SPP along the propagation axis, the plasma is extended past the interface to form partially extended sidewalls. Only partial side walls are needed to prevent radiation in space, since the SPP is confined to the vicinity of the interface.

Lateral confinement of the unidirectional SPP improves both the transient and steady-state (pumped) concurrence. Figure 6(b) shows the transient and steady-state concurrence of two qubits initially prepared in state $|4\rangle$. In comparison to Fig. 2(a), it can be seen that lateral confinement increases both the maximum transient concurrence and the steady-state concurrence. Figure 6(c) shows the dynamics of the qubits under external pumping, where $\rho_{11}, \rho_{22}, \rho_{33}$, and ρ_{44} are the probabilities of finding both qubits in the ground state, both qubits in the excited state, the first qubit in the ground state, and the second qubit in the excited state, and vice versa, respectively. Figure 6(d) shows the steady-state concurrence for a wide range of pump values. The behavior is similar to the case of the infinite interface, Fig. 2(d), except that the range of pump

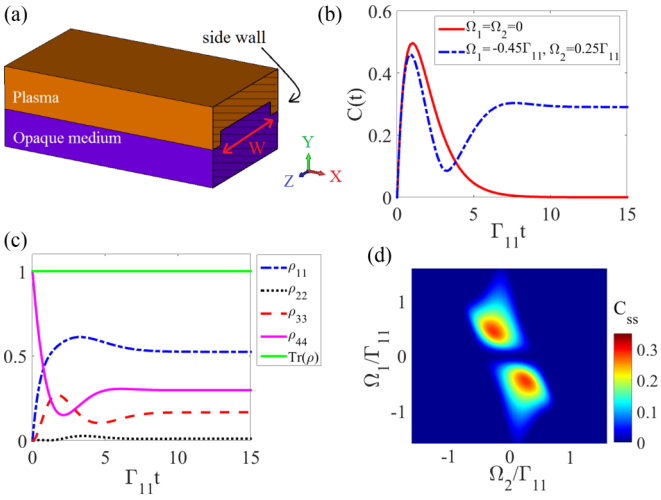

FIG. 6. (a) Finite-width waveguide formed by an opaque medium and biased plasma. (b) Transient and driven concurrence of two qubits interacting through the finite-width waveguide. For the biased plasma, $\omega_p/\omega_0 = 0.95$ and $\omega_c/\omega_0 = 0.21$, and for the opaque medium $\varepsilon = -2$. (c) Dynamics of the qubits under external pumping. (d) Steady-state concurrence for different pump values. Waveguide width is 1.8 μm ($1.2\lambda_0$), qubit separation is 2.4 μm ($1.6\lambda_0$), and $\omega_0/2\pi =$ 200 THz.

values that result in large steady-state concurrence is extended, and the maximum achievable steady-state concurrence is larger in the case of the finite-width waveguide.

In Fig. 7, qubit concurrence is shown for a finite-width waveguide having a defect which spans the entire waveguide width. It can be seen that the concurrence is minimally affected by the defect. Although not shown, as with Fig. 5, in the reciprocal (unbiased) case the defect eliminates the concurrence.

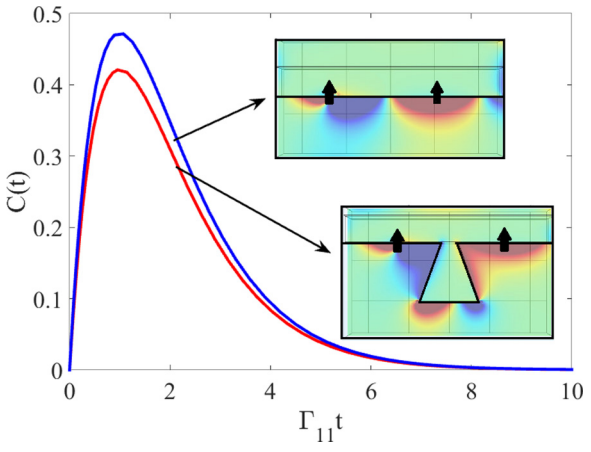

FIG. 7. Transient concurrence of two qubits interacting in a finite-width waveguide [see Fig. 6(a)] consisting of an opaque medium ($\varepsilon = -2$) and a biased plasma ($\omega_p/\omega_0 = 0.95$, $\omega_c/\omega_0 = 0.21$). The defect contour length is of the order of a free-space wavelength, and spans the width of the waveguide, $W = 1.8$ μm ($1.2\lambda_0$). Qubit spacing for the flat interface is 2.4 μm ($1.6\lambda_0$), and for the interface with defect the line-of-sight spacing is 2.4 μm. The system of qubits is initially prepared in the state $|4\rangle = |e_1, g_2\rangle$ and $\omega_0/2\pi = 200$ THz.

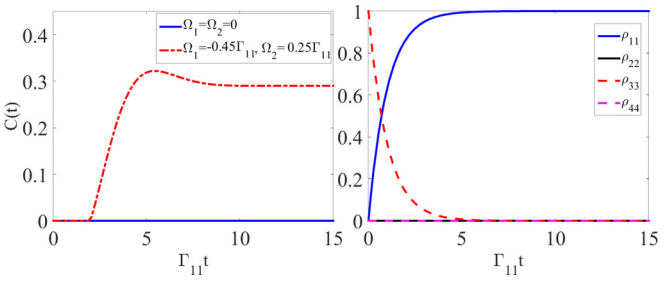

FIG. 8. Left panel: Transient and driven concurrence for a system of qubits interacting through a right going unidirectional SPP while the initial excitation is in the right qubit. Right panel: Dynamics of the qubit system for the transient case. For the biased plasma $\omega_p/\omega_0 =$ 0.95 and $\omega_c/\omega_0 = 0.21$, and for the opaque medium $\varepsilon = -2$. The waveguide geometry is shown in Fig. 6(a), qubit separation is 2.4 μm ($1.6\lambda_0$), and $\omega_0/2\pi = 200$ THz.

F. Effect of different initial-state preparations

An interesting behavior of the concurrence arising from having a unidirectional SPP is that, e.g., if the medium supports only a right going SPP, then the initially excited qubit should be the left qubit, otherwise the qubits remain unentangled, as shown in Fig. 8(a) for the unpumped case $\Omega_1 = \Omega_2 = 0$. Figure 8(b) shows the dynamics of the qubits for this unpumped case. It can be seen that ρ_{33}, which is the probability of finding the right qubit in the excited state and the left qubit in the ground state, starts from 1 and then drops rapidly. However, ρ_{44}, which is the probability of finding the excitation in the left qubit with the right qubit in the ground state, is always zero, meaning that the excitation lost from the right qubit never gets captured by the left qubit. This behavior is particular to a unidirectional environment, and allows for keeping two qubits disentangled at any qubit separation, even if one of them carries an excitation.

However, by applying an external pump we can achieve nonzero concurrence, as also depicted in Fig. 8(a).

The pump is turned on at $t = 0$, and instead of immediately becoming nonzero, the concurrence remains zero for a period of time, then starts rising as a sudden birth in concurrence and reaches a nonzero steady-state value. This delayed sudden birth is quite different from the pumped reciprocal case.

It is also possible to consider different initial states which can give other possible unidirectional SPP assisted dynamical evolutions. Figure 9 shows the case of the initial state being the maximally entangled Bell state $|\Psi_{\text{Bell}}\rangle = (|1\rangle + |2\rangle)/\sqrt{2}$.

We consider that the qubits are interacting through the finite-width waveguide depicted in Fig. 6(a). Figure 9(a) shows the time evolution of the concurrence for both pumped and nonpumped cases. In contrast to the previous cases, the concurrence starts from one due to the maximum degree of entanglement of the initial Bell state. For the nonpumped case the concurrence diminishes in time as the system becomes disentangled, resulting in a sudden death of entanglement. It remains zero for a period of time, then the entanglement experiences a rebirth before decaying exponentially at long times. For the externally pumped case, the concurrence exponentially decays but the qubits do not become completely disentangled. Figure 9(b) shows the dynamics of the qubits

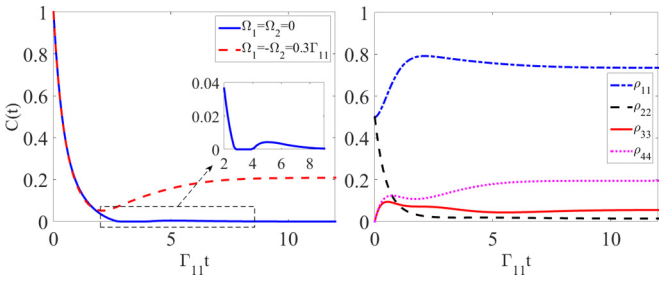

FIG. 9. Left panel: Transient and driven concurrence for a system of qubits initially prepared in the Bell state. Right panel: Dynamics of the qubits system under external pumping. For the biased plasma, $\omega_p/\omega_0 = 0.95$ and $\omega_c/\omega_0 = 0.21$, and for the opaque medium $\varepsilon = -2$. The waveguide geometry is shown in Fig. 6(a) with $W = 1.8\ \mu$m ($1.2\lambda_0$), qubit separation is 2.4 μm ($1.6\lambda_0$), and $\omega_0/2\pi = 200$ THz.

for the pumped case. The population probabilities ρ_{11} and ρ_{22} start from 0.5 due to the Bell state preparation. An interesting behavior in the qubit dynamics is the unequal steady-state values ρ_{33} and ρ_{44} values under pumping with equal intensities $|\Omega_1| = |\Omega_2|$ (in the reciprocal case, $\rho_{33} = \rho_{44}$).

G. Lossy biased plasma

In a lossy medium the SPP loses power as it propagates along the interface, resulting in weaker qubit entanglement. In order to study the effect of loss, we suppose the qubits are interacting through an infinitely wide interface as considered in Fig. 2, but for three different collision frequencies: $\nu = 0$ and $\nu/2\pi = 270$ and 500 MHz. Qubits are initially prepared in the state $|4\rangle = |e_1\rangle \otimes |g_2\rangle$. Figure 10, left panel, shows the transient concurrence. Increasing the collision frequency reduces the concurrence, and for collision frequencies greater than 500 MHz loss dominates the system and an entangled state is not achievable for this relatively wide qubit separation of $1.6\lambda_0$.

The right panel of Fig. 10 shows the steady-state concurrence of the pumped system versus pumping intensity. In comparison to the lossless case [Fig. 2(d)], the range of pump intensities that give nonzero steady-state concurrence has decreased, and the maximum achievable concurrence value is diminished compared to the lossless case.

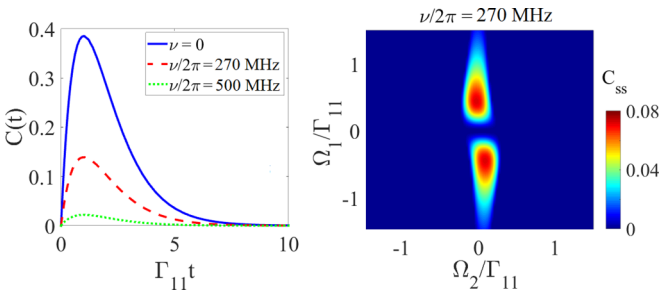

FIG. 10. Left panel: Transient concurrence of two qubits interacting through an infinite interface between a biased plasma ($\omega_p/\omega_0 = 0.95$ and $\omega_c/\omega_0 = 0.21$) and an opaque medium ($\varepsilon = -2$) for different values of the collision frequency. Right panel: Steady-state concurrence for different pump values in the lossy case. Qubit separation is 2.4 μm ($1.6\lambda_0$) and $\omega_0/2\pi = 200$ THz.

IV. CONCLUSIONS

We have derived a master equation for qubit dynamics in a general three-dimensional, nonreciprocal, inhomogeneous, and lossy environment. Spontaneous and pumped entanglement were investigated for two qubits in the vicinity of a photonic topological insulator interface, which supports a nonreciprocal (unidirectional), scattering-immune surface-plasmon polariton in the band gap of the bulk material. We have illustrated the topological nature of the entanglement, and it was shown that large defects in the interface do not impact entanglement for the PTI case, whereas a defect has considerable effect for the reciprocal case. Several initial qubit states were considered, as well as the influence of pump intensity and material loss. Particularities arising from the unidirectional nature of the qubit communication were highlighted.

ACKNOWLEDGMENT

The authors would like to thank S. Buhmann for helpful discussions.

APPENDIX A: MASTER EQUATION DERIVATION AND APPROXIMATIONS

Starting with Eqs. (1)–(5), we note that the nonreciprocal Green's tensor has the following useful property [40]:

$$2i\frac{\omega^2}{c^2}\int d^3\mathrm{r}''\mathbf{G}(\mathbf{r},\mathbf{r}'',\omega)\cdot\mathbf{T}(\mathbf{r}'',\omega)\cdot\mathbf{T}^\dagger(\mathbf{r}'',\omega)\mathbf{G}^*(\mathbf{r}',\mathbf{r}'',\omega)$$
$$=\mathbf{G}(\mathbf{r},\mathbf{r}',\omega)-\mathbf{G}^\dagger(\mathbf{r},\mathbf{r}',\omega). \tag{A1}$$

Under the dipole approximation, the governing Hamiltonian of a system of qubits (two-level atoms) interacting with the surrounding environment can be written as

$$\mathrm{H}=\int d^3\mathbf{r}\int_0^\infty d\omega\hbar\omega\hat{\mathbf{f}}^\dagger(\mathbf{r},\omega)\hat{\mathbf{f}}(\mathbf{r},\omega)+\sum_i\hbar\omega_i\hat{\sigma}_i^\dagger\sigma_i$$
$$-\sum_i\int_0^\infty d\omega[\hat{\boldsymbol{d}}_i\cdot\mathbf{E}(\mathbf{r}_i,\omega)+\mathrm{H.c.}], \tag{A2}$$

where the right side can be decomposed into the reservoir Hamiltonian H_r (first term), the qubit Hamiltonian H_s (second term), and the interaction Hamiltonian H_{sr} (third term). We can modify the total Hamiltonian to include the coherent drive (external laser pump) Hamiltonian V^{AF}, given later [Eq. (10)]. We transform to a frame rotating with the laser frequency ω_l [$\mathrm{H}\rightarrow\hat{\mathrm{U}}^\dagger(t)\mathrm{H}\hat{\mathrm{U}}(t),\hat{\mathrm{U}}(t)=e^{-i\omega_l\sum_i\sigma_i^\dagger\sigma_i t}$] and write the total density matrix of the qubit system and reservoir according to the Schrö dinger equation $\partial_t\rho_T=-i[\mathrm{H},\rho_T]/\hbar$, then we transform to the interaction picture [$\hat{\mathrm{O}}_I=\hat{\mathrm{U}}^\dagger(t)\mathrm{H}\hat{\mathrm{U}}(t),\hat{\mathrm{U}}(t)=e^{-i(\mathrm{H}_s+\mathrm{H}_r)t/\hbar}$] where $\partial_t\rho_{T,I}=-i[\mathrm{H}_I,\rho_{T,I}]$ with $\mathrm{H}_I=\mathrm{H}_{sr,I}$. We integrate to find

$$\rho_{T,I}=\rho_I(0)\mathrm{R}_0+\frac{-i}{\hbar}\int_0^t dt'[\mathrm{H}_I(t'),\rho_{T,I}(t')] \tag{A3}$$

where R_0 is the initial reservoir density matrix. In the interaction picture, by considering $\Gamma_{ii}\ll\omega$ for optical frequencies we make the rotating wave approximation (RWA) in H_I and drop the rapidly varying counter-rotating terms proportional

to $\sigma^\dagger(t')\mathbf{f}^\dagger(\mathbf{r}',\omega)e^{i(\omega_l+\omega)t'}$ and its Hermitian conjugate. The interaction Hamiltonian in the interaction picture reduces to

$$\mathrm{H}_I(t) = -\sum_i \left(\int_0^\infty d\omega \sigma_i^\dagger(t) \boldsymbol{d}_i \cdot \mathbf{E}(\mathbf{r}_i,\omega) e^{-i(\omega-\omega_l)t} + \mathrm{H.c.} \right). \tag{A4}$$

To find the system density matrix we insert Eq. (A3) into the interaction picture Schrö dinger equation and trace over the reservoir:

$$\partial_t \rho_I = \mathrm{Tr}_R \left\{ \frac{-i}{\hbar} [\mathrm{H}_I, \rho_I(0)\mathrm{R}_{0,I}] \right\} - \frac{1}{\hbar^2} \int_0^t dt' \mathrm{Tr}_R\{[\mathrm{H}_I(t),[\mathrm{H}_I(t'),\rho_{T,I}(t')]]\}. \tag{A5}$$

Aside from the rotating wave approximation, we apply a number of other approximations to the density matrix to simplify this further (see Appendix A). We first take the mean initial system reservoir coupling to be zero such that $\mathrm{Tr}_R\{\frac{-i}{\hbar}[\mathrm{H}_I,\rho_I(0)\mathrm{R}_{0,I}]\} = 0$. Then we apply the Born approximation, which states that the reservoir will be largely unaffected by its interaction by the system. Next, we assume that the evolution of the density matrix only depends on its current state (Born-Markov approximation). The Born-Markov approximation comes from the assumption that the reservoir relaxation time is much faster than the relaxation time of the system, and so the memory effect of the reservoir can be ignored. Lastly, we make a second Markov approximation, extending the upper limit of the time integral to infinity to produce a fully Markovian equation. With these simplifications we have

$$\partial_t \rho_I = -\frac{1}{\hbar^2} \int_0^\infty dt' \mathrm{Tr}_R\{[\mathrm{H}_I(t),[\mathrm{H}_I(t-t'),\rho_I(t)\mathrm{R}_0]]\}. \tag{A6}$$

We suppose that the atomic transition frequency of the qubits is ω_0. Then, for the first term in Eq. (A6) we have

$$\mathrm{Tr}_R\{\mathrm{H}_I(t)\mathrm{H}_I(t-t')\rho_I(t)\mathrm{R}_0\} = \sum_{i,j} d_{\alpha i} d_{\beta j} \int_0^\infty d\omega e^{i(\omega_0-\omega)t'} \sigma_i^\dagger \sigma_j \rho_{T,I} \mathrm{Tr}_R \times (\hat{\mathrm{E}}_\alpha(\mathbf{r}_i,\omega)\hat{\mathrm{E}}_\beta^\dagger(\mathbf{r}_j,\omega)\mathrm{R}_0) \tag{A7}$$

where

$$\sigma_i = |g_i\rangle\langle e_i|, \sigma_i{}^\dagger = |e_i\rangle\langle g_i| \tag{A8}$$

are the atomic lowering and raising operators describing energy-level transitions for each qubit, and where it is supposed that one of the qubits is polarized along α and the other one is polarized along β. Considering Eq. (5) for the nonreciprocal Green's tensor and $\mathrm{Tr}_R\{\hat{\mathbf{f}}(r,\omega)\hat{\mathbf{f}}^\dagger(r',\omega')\mathrm{R}_0\} = (\bar{n}(\omega)+1)\delta(r-r')\delta(\omega-\omega')$ with zero thermal photon occupation $\bar{n}(\omega) = 0$, it can be easily shown that

$$\mathrm{Tr}_R[\mathrm{E}_\alpha(\mathbf{r}_i,\omega)\mathrm{E}_\beta^\dagger(\mathbf{r}_j,\omega)\mathrm{R}_0] = \frac{\hbar}{\pi\varepsilon_0}\frac{\omega^4}{c^4} \int d^3\mathbf{r} \mathrm{G}_{\alpha\gamma}(\mathbf{r}_i,\mathbf{r},\omega) \times \left[\frac{\varepsilon_{\gamma\gamma'}(\mathbf{r},\omega) - \varepsilon_{\gamma\gamma'}^\dagger(\mathbf{r},\omega)}{2i} \right] \mathrm{G}_{\gamma'\beta}^*(\mathbf{r}_j,\mathbf{r},\omega) = \frac{\hbar}{2i\pi\varepsilon_0}\frac{\omega^2}{c^2}[\mathrm{G}_{\alpha,\beta}(\mathbf{r}_i,\mathbf{r}_j,\omega) - \mathrm{G}_{\beta,\alpha}^*(\mathbf{r}_j,\mathbf{r}_i,\omega)]. \tag{A9}$$

Thus, we have

$$\mathrm{Tr}_R\{\mathrm{H}_I(t)\mathrm{H}_I(t-t')\rho_I(t)\mathrm{R}_0\} = \frac{\hbar}{2i\pi\varepsilon_0 c^2} \sum_{i,j} \sigma_i^\dagger \sigma_j \rho_I(t) \times \int_0^\infty [d_{\alpha i}\mathrm{G}_{\alpha\beta}(\mathbf{r}_i,\mathbf{r}_j,\omega)d_{\beta j} - d_{\beta j}\mathrm{G}_{\beta\alpha}^*(\mathbf{r}_j,\mathbf{r}_i,\omega)d_{\alpha i}] \times \omega^2 d\omega e^{i(\omega_0-\omega)t'}. \tag{A10}$$

Following the same procedure for the second term in Eq. (A6),

$$\mathrm{Tr}_R\{\mathrm{H}_I(t-t')\rho_I(t)\mathrm{R}_0\mathrm{H}_I(t)\} = \frac{\hbar}{2i\pi\varepsilon_0 c^2} \sum_{i,j} \sigma_j \rho_I(t) \sigma_i^\dagger \times \int_0^\infty [d_{\beta i}\mathrm{G}_{\beta\alpha}(\mathbf{r}_i,\mathbf{r}_j,\omega)d_{\alpha j} - d_{\alpha j}\mathrm{G}_{\alpha\beta}^*(\mathbf{r}_j,\mathbf{r}_i,\omega)d_{\beta i}] \times \omega^2 d\omega e^{i(\omega_0-\omega)t'}. \tag{A11}$$

Replacing Eqs. (A10) and (A11) in Eq. (A6) and performing the time integral over t' gives the evolution of the density matrix in the interaction picture, where we have used the Kramers-Kronig relation

$$\mathcal{P}\int_{-\infty}^\infty \frac{\mathrm{ReG}_{\alpha\beta}}{\omega-\omega_0} d\omega = -\pi \mathrm{ImG}_{\alpha\beta}, \quad \mathcal{P}\int_{-\infty}^\infty \frac{\mathrm{ImG}_{\alpha\beta}}{\omega-\omega_0} d\omega = \pi \mathrm{ReG}_{\alpha\beta}. \tag{A12}$$

Transforming back to the Schrödinger picture, we obtain the master equation for the two-level system dynamics Eqs. (6) and (7).

Next, we briefly discuss the approximations used in the derivation of the master equations (6) and (7).

The first approximation made in the derivation is the RWA where in the interaction picture we drop the rapidly varying counter-rotating terms in H_I. This approximation is valid for $\Gamma_{ii} \ll \omega_0$. The qubit transition frequency is $\omega_0/2\pi =$ 200 THz, and we assume a dipole moment $d = 60$ D. For an interface made of lossless biased plasma, $\Gamma_{ii}/2\pi \sim 450$ MHz, and, for the lossy biased plasma with $\nu/2\pi = 500$ MHz, $\Gamma_{ii}/2\pi \sim 2$ GHz. For the non-biased-plasma–opaque-medium interface (interface supporting reciprocal SPP) $\Gamma_{ii}/2\pi \sim 75$ MHz. In all cases the condition for the validity of the RWA is strongly met.

We also applied the Born-Markov approximation, which comes from the assumption that the reservoir relaxation time, τ_R, is much faster than the relaxation time of the qubit system $\tau_S = 1/\Gamma_{ii}$. This allows for the expansion of the exact equation of motion for the density matrix up to second order, and makes the quantum master equation local in time. For a nonreciprocal

medium the fluctuation-dissipation theorem [40] is

$$\langle \mathrm{P}_\alpha(\omega,\mathbf{r})\mathrm{P}^\dagger_\alpha(\omega',\mathbf{r}')\rangle = \frac{\hbar}{4i}[\boldsymbol{\varepsilon}(\omega,\mathbf{r}) - \boldsymbol{\varepsilon}^\dagger(\omega,\mathbf{r})]\mathrm{N}(\omega,\mathrm{T}) \times \delta(\omega-\omega')\delta(\mathbf{r}-\mathbf{r}')\delta_{\alpha\beta}, \quad \text{(A13)}$$

where $\mathrm{N}(\omega,\mathrm{T}) = 2/[\exp(\hbar\omega/k_B\mathrm{T}) - 1]$ for negative frequencies and $\mathrm{N}(\omega,\mathrm{T}) = 1 + 2/[\exp(\hbar\omega/k_B\mathrm{T}) - 1]$ for positive frequencies, where k_B is Boltzmann's constant. Regarding $\mathbf{E}(\mathbf{r},\omega) = (\omega^2/c^2\varepsilon_0)\int_V d\mathbf{r}'\mathbf{G}(\mathbf{r},\mathbf{r}',\omega)\cdot\mathbf{P}(\mathbf{r}',\omega)$, it can be shown that

$$\langle \mathrm{E}_\alpha(\mathbf{r},\omega)\mathrm{E}^\dagger_\alpha(\mathbf{r},\omega)\rangle = \mathrm{k}_0^2\frac{\hbar}{4i\varepsilon_0^2}\mathrm{N}(\omega,\mathrm{T}) \times [\mathrm{G}_{\alpha\alpha}(\mathbf{r},\mathbf{r},\omega) - \mathrm{G}^\dagger_{\alpha\alpha}(\mathbf{r},\mathbf{r},\omega)], \quad \text{(A14)}$$

which reduces in the reciprocal case to

$$\langle \mathrm{E}_\alpha(\mathbf{r},\omega)\mathrm{E}^\dagger_\alpha(\mathbf{r},\omega)\rangle = \frac{\hbar\mathrm{k}_0^2}{2\varepsilon_0^2}\mathrm{N}(\omega,\mathrm{T})\mathrm{Im}[\mathrm{G}_{\alpha\alpha}(\mathbf{r},\mathbf{r},\omega)]. \quad \text{(A15)}$$

The bath relaxation time can be estimated by looking at the decay time of the correlation

$$\langle \mathrm{E}_\alpha(\mathbf{r},t)\mathrm{E}^\dagger_\alpha(\mathbf{r},0)\rangle = \frac{1}{2\pi}\int_{-\infty}^{+\infty} d\omega e^{-i\omega t}\langle \mathrm{E}_\alpha(\mathbf{r},\omega)\mathrm{E}^\dagger_\alpha(\mathbf{r},\omega)\rangle. \quad \text{(A16)}$$

The Green's function consists of homogeneous (vacuum) and scattered terms, and τ_R will be dominated by the slower scattered field contribution [for the vacuum term, $\tau_R(T) = \hbar/\pi k_B T$ [47], so that $\tau_R(300K) \sim 10$ fs]. For the scattered part of the Green's function for an interface made of nonbiased plasma and an opaque medium (interface supporting reciprocal SPP), using the Green's function in [48], $\tau_R \sim 10^{-11}$ s for $\nu = 500$ and 270 MHz, whereas $\tau_S = 1/\Gamma_{ii} \sim 10^{-8}$ s, so that we can ignore the reservoir relaxation time.

APPENDIX B: COMPARISON WITH PREVIOUS 1D CHIRAL THEORY AND WITH 2D AND 3D GREEN'S FUNCTIONS

Here we discuss the relation between the general ME we derived in terms of the exact electromagnetic Green's function, resulting, for two qubits, in the Lindblad Eq. (11), and the 1D phenomenological ME for two-level systems coupled to a 1D chiral reservoir presented in [18,21] (see also [17,20]). The 1D chiral theory is based on the notion of right and left, defining couplings $\gamma_{\mathrm{R,L}}$, whereas the theory presented here is based on qubit interactions Γ_{ij}; note that Γ_{ij} plays the role of a Γ_{right} if $x_i > x_j$, but plays the role of Γ_{left} if $x_i < x_j$. To facilitate the comparison with the 1D chiral theory we will assume two qubits with positions x_1 and x_2, with $x_2 > x_1$. In [18,21] phenomenological quantities γ_{iR},γ_{1L} for $i = 1,2$ are utilized, and setting $\gamma_{1R} = \gamma_{2R} = \gamma_R$ and $\gamma_{1L} = \gamma_{2L} = \gamma_L$, the 1D chiral Lindblad superoperator is

$$\begin{aligned}\mathcal{L}\rho_s(t) = &\sum_{j=1,2}\gamma_j(2\sigma_j\rho_s\sigma_j^\dagger - \rho_s\sigma_j^\dagger\sigma_j - \sigma_j^\dagger\sigma_j\rho_s)\\ &+\gamma_R e^{ik_R(x_2-x_1)}(\sigma_2\rho_s\sigma_1^\dagger - \rho_s\sigma_1^\dagger\sigma_2)\\ &+\gamma_R e^{-ik_R(x_2-x_1)}(\sigma_1\rho_s\sigma_2^\dagger - \sigma_2^\dagger\sigma_1\rho_s)\\ &+\gamma_L e^{-ik_L(x_2-x_1)}(\sigma_1\rho_s\sigma_2^\dagger - \rho_s\sigma_2^\dagger\sigma_1)\\ &+\gamma_L e^{ik_L(x_2-x_1)}(\sigma_2\rho_s\sigma_1^\dagger - \sigma_1^\dagger\sigma_2\rho_s), \end{aligned} \quad \text{(B1)}$$

where $k_{L,R} = \omega_0/v_{gL,R}$, with v_g being the group velocity of the guided photons.

If we assume now a plasmonic environment, the total emission of the source can be divided into several decay channels: $\Gamma_{11} = \Gamma_{\mathrm{r}} + \Gamma_{\mathrm{nr}} + \Gamma_{\mathrm{SPP}}$, where Γ_{r} represents free-space radiation, Γ_{nr} represents losses in the material (quenching), and Γ_{SPP} represents excitation of SPPs. Material absorption and radiation do not contribute to strong qubit-qubit interactions, and therefore we are interested in systems with strong decay through the plasmon channel, Γ_{SPP}, where the fraction of all emissions that are coupled to plasmons is expressed by $\beta_{ij} = \Gamma_{ij,\mathrm{SPP}}/\Gamma_{11}$, with $i \neq j$.

Assuming a plasmonic environment with a preferred propagation axis, here taken as x, in order to connect our formulation with previous 1D chiral formulations [18,21] we introduce a particular 1D plasmonic version of Eq. (8):

$$\begin{aligned} g_{ij} &\simeq g_{ij,\mathrm{SPP}} = \beta_{ij}\Gamma_{11}e^{-\mathrm{k}''_{\mathrm{ij}}|\mathrm{x}_i-\mathrm{x}_j|}\sin[\mathrm{k}'_{\mathrm{ij}}(\mathrm{x}_i-\mathrm{x}_j)],\\ \Gamma_{ij} &\simeq \Gamma_{ij,\mathrm{SPP}}\\ &= \begin{cases}(\beta_{12}+\beta_{21})\Gamma_{11}, & i=j\\ 2\beta_{ij}\Gamma_{11}e^{-\mathrm{k}''_{\mathrm{ij}}|\mathrm{x}_i-\mathrm{x}_j|}\cos[\mathrm{k}'_{\mathrm{ij}}(\mathrm{x}_i-\mathrm{x}_j)], & i\neq j,\end{cases}\end{aligned} \quad \text{(B2)}$$

where $\mathrm{k}_{\mathrm{ij}} = \mathrm{k}_{\mathrm{spp,ij}} = \mathrm{k}'_{\mathrm{spp,ij}} + i\mathrm{k}''_{\mathrm{spp,ij}}$ are the SPP wave numbers. In the systems considered here the bulk modes are reciprocal, whereas the interface SPP is strongly nonreciprocal (unidirectional). Thus, to compare with the 1D chiral ME it is sensible to consider the SPP (nonreciprocal) contribution.

As defined in Eq. (B2), $\Gamma_{ij,\mathrm{SPP}}$ is discontinuous at $x_i = x_j$ in the nonreciprocal case, i.e., $\Gamma_{ij,\mathrm{SPP}} = 2\beta_{ij}\Gamma_{11}$ as $|x_i \to x_j|$, whereas at $x_i = x_j$, $\Gamma_{ij,\mathrm{SPP}} = (\beta_{12}+\beta_{21})\Gamma_{11}$. As we show below, the SPP contribution in the considered PTI system is indeed discontinuous at $x_i = x_j$. However, the exact Γ_{ij}, which contains both the SPP and radiation continuum, is continuous at the source point even in the nonreciprocal case. As another example of this, a 3D analytical Green's function for a nonreciprocal bulk medium is provided in [49] [see their Eq. (117)], where Γ_{ij} is also seen to be continuous.

Equating Eq. (11) in the 1D case [i.e., using Eq. (B2)] and Eq. (B1) term by term, the two Lindblad superoperators will be equal if

$$\gamma_j = \frac{\Gamma_{jj}}{2}, \quad \text{(B3)}$$

$$\gamma_R e^{\pm ik(x_2-x_1)} = \frac{\Gamma_{21}}{2} \pm ig_{21}, \quad \text{(B4)}$$

$$\gamma_L e^{\pm ik(x_1-x_2)} = \frac{\Gamma_{12}}{2} \pm ig_{12}. \quad \text{(B5)}$$

If we now make the assignments

$$\beta_{21}\Gamma_{11} \to \gamma_R, \quad \beta_{12}\Gamma_{11} \to \gamma_L, \quad \text{(B6)}$$

$$\mathrm{k}_{\mathrm{spp,12}} \to \frac{\omega_0}{v_{gL}}, \quad \mathrm{k}_{\mathrm{spp,21}} \to \frac{\omega_0}{v_{gR}}, \quad \text{(B7)}$$

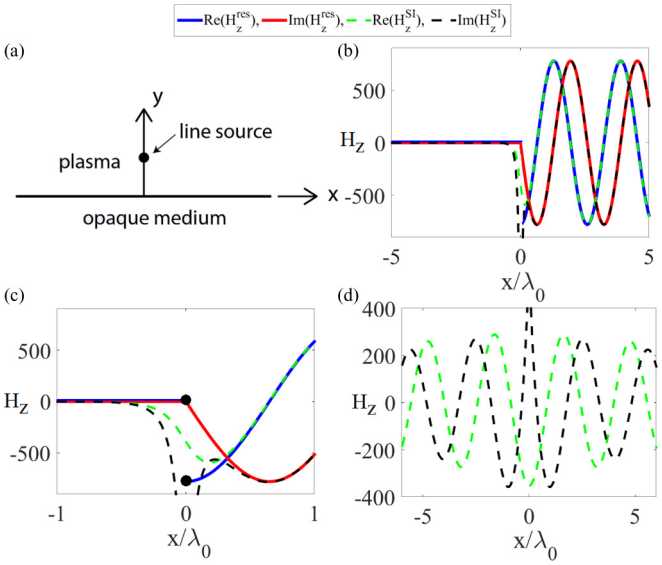

FIG. 11. (a) Magnetic current source (black dot, z directed and z invariant) located at $x = 0, y = d$ inside a biased-plasma region, with an opaque half space occupying $y < 0$. (b) Magnetic field $\mathrm{H}_z(x)$ at the interface of an $\varepsilon = -2$ half space and a magnetized plasma having $\omega_p/\omega_0 = 0.95$ and $\omega_c/\omega_0 = 0.21$, at $\omega_0/2\pi = 200$ THz. The magnetic line source is located $\lambda_0/10$ above the interface in the plasma region, and the field is evaluated at $(x, y = \lambda_0/10, z = 0)$. (c) Field behavior in the vicinity of the source showing the discontinuity of the residue component. (d) Same as panel (b) for the unbiased (reciprocal) case, $\omega_c/\omega_0 = 0$.

then Eqs. (B3)–(B5) are satisfied and Eq. (11) becomes strictly equal to Eq. (B1). It is worth stressing that physically the two formulations still differ, since Eq. (B7) is not exact (phase velocity and group velocity are different quantities). Nonetheless it is interesting to try to connect the phenomenological parameters in the model Eq. (B1) to the corresponding ones in Eq. (11), which are obtained in terms of the Green's function, and hence can be computed for arbitrary environments.

Using the rates defined in Eq. (B2), Eq. (12) reduces to

$$\mathcal{C}^{1\mathrm{D}}(t) = 2\beta_{21}\Gamma_{11}e^{-k''_{\mathrm{spp}}|x_2-x_1|}te^{-\Gamma_{11}t}, \tag{B8}$$

which is distance independent in the lossless case, as noted in [18] [using Eq. (B6), Eq. (B8) is the same as Eq. (6) in [18]].

1. Discontinuity of the SPP and 2D Green's function

Here we show that for the strongly nonreciprocal (unidirectional) case, and for a general nonreciprocal case, near the source point the SPP contribution to the Green's function is discontinuous. We also show that for nonreciprocal systems, $\Gamma_{21} > \Gamma_{11}$ can occur.

To avoid analytical complications of the general 3D case, we first assume a simple 2D model of a z-directed and z-invariant magnetic current source located at $x = 0, y = d$ inside a biased-plasma half space, adjacent to an opaque half space occupying $y < 0$, as depicted in Fig. 11(a). The resulting magnetic field in the plasma is [50,51]

$$\mathrm{H}_z = \mathrm{H}_z^{\mathrm{inc}} + \frac{\mathrm{A}_0}{2\pi}\int_{-\infty}^{+\infty}\frac{1}{2\gamma_p}\mathrm{R}_0\, e^{-\gamma_p(y+d)+i\mathrm{k}_x x}d\mathrm{k}_x, \tag{B9}$$

where $\mathrm{A}_0 = i\omega\varepsilon_0\varepsilon_{\mathrm{eff}}\mathrm{I}_m$, where I_m is the magnetic current (set to unity) and R_0 accounts for the interface,

$$\mathrm{R}_0 = \frac{\frac{\gamma_p}{\varepsilon_{\mathrm{eff}}} + \frac{i\varepsilon_{12}}{\varepsilon_{11}}\frac{i\mathrm{k}_x}{\varepsilon_{\mathrm{eff}}} - \frac{\gamma_m}{\varepsilon_m}}{\frac{\gamma_p}{\varepsilon_{\mathrm{eff}}} - \frac{i\varepsilon_{12}}{\varepsilon_{11}}\frac{i\mathrm{k}_x}{\varepsilon_{\mathrm{eff}}} + \frac{\gamma_m}{\varepsilon_m}}, \tag{B10}$$

where $\gamma_p = \sqrt{\mathrm{k}_x^2 - \varepsilon_{\mathrm{eff}}\mathrm{k}_0^2}$, $\gamma_m = \sqrt{\mathrm{k}_x^2 - \varepsilon_m\mathrm{k}_0^2}$, and ε_m is the permittivity of the metal (opaque medium). The field in the absence of the interface is

$$\begin{aligned}\mathrm{H}_z^{\mathrm{inc}} &= \frac{\mathrm{A}_0}{2\pi}\int_{-\infty}^{+\infty}\frac{1}{2\gamma_p}e^{-\gamma_p|y-d|+i\mathrm{k}_x x}d\mathrm{k}_x \\ &= \frac{\mathrm{A}_0}{-4i}\mathrm{H}_0^{(1)}(\mathrm{k}_0\sqrt{\varepsilon_{\mathrm{eff}}}\rho)\end{aligned} \tag{B11}$$

where $\mathrm{H}_0^{(1)}$ is the Hankel function of the first kind and order zero and $\rho = \sqrt{x^2 + (y-d)^2}$. The source-point singularity is contained in $\mathrm{Im}(\mathrm{H}_0^{(1)})$, and $\Gamma \sim \mathrm{Im}(\mathrm{G}_{yy}) \sim \mathrm{Re}(\mathrm{E}_y) \sim \mathrm{Re}(\mathrm{H}_z)$.

The interface reflection coefficient R_0, leading to the scattered field, contains pole singularities at the SPP wave numbers (e.g., the denominator of R_0 is the SPP dispersion equation). For $|\varepsilon_m| \to \infty$ (perfect conductor), there is one pole at $k_{\mathrm{spp},x} = \pm k_0\sqrt{\varepsilon_{11}}$ for $\omega_c \gtrless 0$. For $|\varepsilon_m|$ finite the dispersion equation must be solved numerically, and the plasma may be strongly nonreciprocal, supporting a unidirectional SPP (operating in the bulk band gap), nonreciprocal supporting SPPs traveling in opposite directions with unequal wave numbers (operating above the bulk band gap), or, in the unbiased (no band gap) case, reciprocal.

Complex-plane analysis of the magnetic field leads to its evaluation as the sum of a branch cut integral (continuous spectrum) and a discrete residue (SPP) contribution, the latter being

$$\begin{aligned}\mathrm{H}_z^{\mathrm{res}} &= \theta(-x)i\mathrm{A}_0\,\mathrm{Res}^{(-)}\frac{e^{-\gamma_p^{(-)}(y+d)+i\mathrm{k}_{x,\mathrm{SPP}}^{(-)}x}}{2\gamma_p^{(-)}} \\ &+ \theta(x)i\mathrm{A}_0\mathrm{Res}^{(+)}\frac{e^{-\gamma_p^{(+)}(y+d)+i\mathrm{k}_{x,\mathrm{SPP}}^{(+)}x}}{2\gamma_p^{(+)}}\end{aligned} \tag{B12}$$

where $\mathrm{Res}^{(\pm)}$ is the residue of R_0 evaluated at $\mathrm{k}_x = \mathrm{k}_{x,\mathrm{SPP}}^{(\pm)}$, and $\gamma_p^{(\pm)} = \sqrt{\left(\mathrm{k}_{x,\mathrm{SPP}}^{(\pm)}\right)^2 - \epsilon_{\mathrm{eff}}\mathrm{k}_0^2}$, where $\mathrm{k}_{x,\mathrm{SPP}}^{(\pm)}$ is the SPP pole for $\mathrm{k}_x \gtrless 0$ (forward propagating or backward propagating), and where $\theta(x)$ is the Heaviside step function. In the strongly nonreciprocal (unidirectional) case, only one pole is present, leading to only one term in Eq. (B12).

Figure 11(b) shows the magnetic field in the bulk band gap for $\omega_c > 0$ obtained by numerical evaluation of the Sommerfeld integral (B9), and by assuming only the residue component Eq. (B12) (since we operate in the bulk band gap and the gap Chern number is -1, then there is one unidirectional SPP). The opaque medium is topologically trivial, and is an unbiased plasma having $\varepsilon = -2$. As shown in the inset to Fig. 11(c), the residue accurately approximates the field except very close to the source, where the real

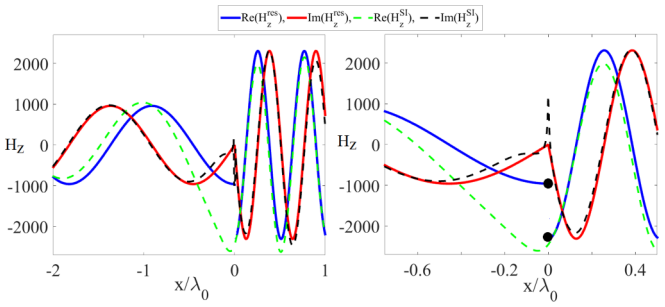

FIG. 12. (a) Magnetic field $H_z(x)$ at the interface of an $\varepsilon = -0.47$ half space and a magnetized plasma having $\omega_p/\omega_0 = 0.82$ and $\omega_c/\omega_0 = 0.17$ where $\omega_0/2\pi = 230$ THz. The magnetic line source is located $\lambda_0/10$ above the interface in the plasma region, and the field is evaluated at $(x, y = \lambda_0/10, z = 0)$. (b) Field behavior in the vicinity of the source showing the discontinuity of the residue component.

part of the residue ($\propto \Gamma_{SPP}$) has an unphysical discontinuity, indicated by the two black dots. In this case, the radiation continuum compensates for the discontinuity of the residue, such that the real part of the full Sommerfeld integral ($\propto \Gamma$) is continuous, and the SPP peak is pushed away from the source point.

As a result of the importance of the radiation continuum near the source, at some points $H_z(x = 0) < H_z(x > 0)$, so that Γ_{21} exceeds Γ_{11}. Figure 11(d) shows the unbiased (reciprocal) case for the full Sommerfeld integral, where the field peak occurs at $x = 0$ and $\Gamma_{21} < \Gamma_{11}$ at all points. In general, there is a quadrature relationship between the dissipative and coherent rates.

Figure 12 shows the magnetic field at a frequency outside the band gap, where we have two SPPs propagating in opposite directions with unequal wave numbers. As with the unidirectional case, the residue shows a discontinuity at the source point.

2. 3D Green's function

Considering now the 3D case of an electric dipole source at the interface, Fig. 13 shows the dissipative decay and coherent rates of Eq. (8) computed using the finite element method (COMSOL, [46]). In this case, it is impossible to separate the discrete and continuum contributions to the field. Figures 13(a) and 13(b) show the rates for qubits at the interface as a function of qubit separation for two frequencies within the band gap, and Fig. 13(c) shows the rates normalized by Γ_{ii} for a fixed separation as a function of height above the interface. It can be seen that, as predicted by the previous analytical 2D model, it occurs that Γ is nearly discontinuous at the source point (the discontinuity of the discrete spectrum is softened by the radiation continuum), and that $\Gamma_{21} > \Gamma_{11}$ at some points. The coherent rate becomes unbounded at the source due to the well-known divergence of the real part of the Green's function.

APPENDIX C: CONCURRENCE IN THE UNIDIRECTIONAL CASE

In this section we derive the concurrence for a unidirectional system.

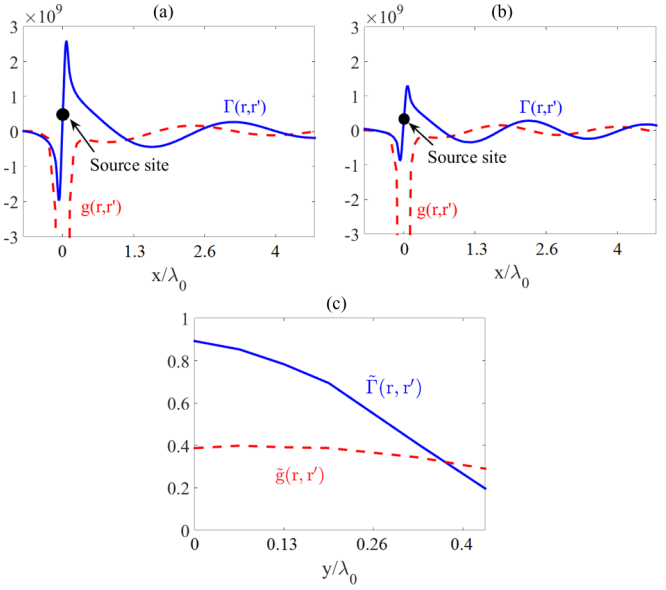

FIG. 13. (a) Dissipative decay (solid blue) and coherent (dashed red) rates at the interface of a biased plasma ($\omega_p/\omega_0 = 0.95$, $\omega_c/\omega_0 = 0.21$) and an opaque medium ($\varepsilon = -2$) at $\omega_0/2\pi = 200$ THz. (b) The same as panel (a) but for 207 THz. The black circle demonstrates the point dipole source, and the dipole moment is $d = 60$ D. (c) The normalized rates as a function of the height of the two qubits above the interface for a fixed separation of 2.1 μm.

Suppose that the system of qubits is communicating through a strongly nonreciprocal environment, so that the communication is strictly unidirectional, such as occurs for SPPs at PTI interfaces. Assuming that $\mathbf{G}(\mathbf{r}_1,\mathbf{r}_2)$ and $\mathbf{G}(\mathbf{r}_2,\mathbf{r}_1)$ are the dyadic Green's function propagators along two opposite directions, the unidirectionality assumption leads to, e.g., $\mathbf{G}(\mathbf{r}_1,\mathbf{r}_2) = 0$ ($\Gamma_{12} = g_{12} = 0$) and $\mathbf{G}(\mathbf{r}_2,\mathbf{r}_1) \neq 0$.

Under this unidirectionality assumption, the 3D Lindblad superoperator (7) reduces to

$$\begin{aligned}\frac{\partial \rho_s(t)}{\partial t} = &-\frac{i}{\hbar}[\mathrm{H}_s + \mathrm{V}^{AF}, \rho_s(t)] \\ &+ \frac{\Gamma_{11}}{2}[2\sigma_1\rho_s(t)\sigma_1^\dagger - \sigma_1^\dagger\sigma_1\rho_s(t) - \rho_s(t)\sigma_1^\dagger\sigma_1] \\ &+ \frac{\Gamma_{11}}{2}[2\sigma_2\rho_s(t)\sigma_2^\dagger - \sigma_2^\dagger\sigma_2\rho_s(t) - \rho_s(t)\sigma_2^\dagger\sigma_2] \\ &+ \left(\frac{\Gamma_{21}}{2} + ig_{21}\right)[\sigma_2\rho_s(t)\sigma_1^\dagger - \rho_s(t)\sigma_1^\dagger\sigma_2] \\ &+ \left(\frac{\Gamma_{21}}{2} - ig_{21}\right)[\sigma_1\rho_s(t)\sigma_2^\dagger - \sigma_2^\dagger\sigma_1\rho_s(t)] \quad \text{(C1)}\end{aligned}$$

where it has been assumed that $\Gamma_{11} = \Gamma_{22}$.

Defining the basis

$$\begin{aligned}&|1\rangle = |g_1\rangle \otimes |g_2\rangle = |g_1, g_2\rangle, \quad |2\rangle = |e_1\rangle \otimes |e_2\rangle = |e_1, e_2\rangle, \\ &|3\rangle = |g_1\rangle \otimes |e_2\rangle = |g_1, e_2\rangle, \quad |4\rangle = |e_1\rangle \otimes |g_2\rangle = |e_1, g_2\rangle \end{aligned} \quad \text{(C2)}$$

and considering the system of qubits to be initially prepared in the state $|4\rangle = |e_1\rangle \otimes |g_2\rangle$, it can be shown that for the nonpumped case the nonzero components of the density matrix

in Eq. (C1) are ($\rho = \rho_s$)

$$\begin{aligned}
\partial_t \rho_{11} &= \Gamma_{11}(\rho_{33} + \rho_{44}) + \gamma\rho_{34} + \gamma^*\rho_{43},\\
\partial_t \rho_{33} &= -\Gamma_{11}\rho_{33} - \gamma\rho_{34} - \gamma^*\rho_{43},\\
\partial_t \rho_{34} &= -\Gamma_{11}\rho_{34} - \gamma^*\rho_{44},\\
\partial_t \rho_{43} &= -\Gamma_{11}\rho_{43} - \gamma\rho_{44},\\
\partial_t \rho_{44} &= -\Gamma_{11}\rho_{44}
\end{aligned} \tag{C3}$$

where $\gamma = \Gamma_{21}/2 + ig_{21}$. For all times the density matrix is block diagonal. Concurrence for arbitrary materials can be calculated as [44]

$$\mathcal{C} = \max(0, \sqrt{u_1} - \sqrt{u_2} - \sqrt{u_3} - \sqrt{u_4}), \tag{C4}$$

where u_i are arranged in descending order of the eigenvalues of the matrix $\rho(t)\rho^y(t)$, where $\rho^y(t) = \sigma_y \otimes \sigma_y \rho^\star(t) \sigma_y \otimes \sigma_y$ is the spin-flip density matrix with σ_y being the Pauli matrix.

We have

$$\rho(t)\rho^y(t) = \begin{bmatrix} 0 & 0 & 0 & 0 \\ 0 & 0 & 0 & 0 \\ 0 & 0 & x & y \\ 0 & 0 & z & x \end{bmatrix} \rightarrow \begin{array}{c} u_1 = x + \sqrt{yz} \\ u_2 = x - \sqrt{yz} \\ u_3 = 0 \\ u_4 = 0 \end{array} \tag{C5}$$

such that $x = |\rho_{34}|^2 + \rho_{33}\rho_{44}$, $y = 2\rho_{34}\rho_{33}$, and $z = 2\rho_{43}\rho_{44}$, and

$$\begin{aligned}
\rho_{44}(t) &= e^{-\Gamma_{11}t},\\
\rho_{43}(t) &= -\gamma t e^{-\Gamma_{11}t},\\
\rho_{34}(t) &= -\gamma^* t e^{-\Gamma_{11}t},\\
\rho_{33}(t) &= |\gamma|^2 t^2 e^{-\Gamma_{11}t},\\
\rho_{11}(t) &= 1 - e^{-\Gamma_{11}t} - |\gamma|^2 t^2 e^{-\Gamma_{11}t},
\end{aligned} \tag{C6}$$

which leads to Eq. (12).

[1] M. A. Nielsen and I. L. Chuang, *Quantum Computation and Quantum Information* (Cambridge University Press, Cambridge, England, 2000).

[2] L. Masanes, S. Pironio, and A. Acin, Secure device-independent quantum key distribution with causally independent measurement devices, Nat. Commun. **2**, 238 (2011).

[3] W. H. Zurek, Decoherence, einselection, and the quantum origins of the classical, Rev. Mod. Phys. **75**, 715 (2003).

[4] M. B. Plenio and S. F. Huelga, Entangled Light from White Noise, Phys. Rev. Lett. **88**, 197901 (2002).

[5] F. Verstraete, M. M. Wolf, and J. I. Cirac, Quantum computation and quantum-state engineering driven by dissipation, Nat. Phys. **5**, 633 (2009).

[6] A. Sarlette, J. M. Raimond, M. Brune, and P. Rouchon, Stabilization of Nonclassical States of the Radiation Field in a Cavity by Reservoir Engineering, Phys. Rev. Lett. **107**, 010402 (2011).

[7] L. Hartmann, W. Dur, and H.-J. Briegel, Steady-state entanglement in open and noisy quantum systems, Phys. Rev. A **74**, 052304 (2006).

[8] H. Krauter, C. A. Muschik, K. Jensen, W. Wasilewski, J. M. Petersen, J. I. Cirac, and E. S. Polzik, Entanglement Generated by Dissipation and Steady State Entanglement of two Macroscopic Objects, Phys. Rev. Lett. **107**, 080503 (2011).

[9] F. Lucas, F. Mintert, and A. Buchleitner, Tailoring many-body entanglement through local control, Phys. Rev. A **88**, 032306 (2013).

[10] B. Bellomo, R. Messina, and M. Antezza, Dynamics of an elementary quantum system in environments out of thermal equilibrium, Europhys. Lett. **100**, 20006 (2012).

[11] B. Bellomo, R. Messina, D. Felbacq, and M. Antezza, Quantum systems in a stationary environment out of thermal equilibrium, Phys. Rev. A **87**, 012101 (2013).

[12] B. Bellomo and M. Antezza, Steady entanglement out of thermal equilibrium, Europhys. Lett. **104**, 10006 (2013).

[13] B. Bellomo and M. Antezza, Creation and protection of entanglement in systems out of thermal equilibrium, New J. Phys. **15**, 113052 (2013).

[14] B. Bellomo and M. Antezza, Nonequilibrium dissipation-driven steady many-body entanglement, Phys. Rev. A **91**, 042124 (2015).

[15] S. Mancini and H. M. Wiseman, Optimal control of entanglement via quantum feedback, Phys. Rev. A **75**, 012330 (2007).

[16] R. N. Stevenson, J. J. Hope, and A. R. R. Carvalho, Engineering steady states using jump-based feedback for multipartite entanglement generation, Phys. Rev. A **84**, 022332 (2011).

[17] P. Lodahl, S. Mahmoodian, S. Stobbe, P. Schneeweiss, J. Volz, A. Rauschenbeutel, H. Pichler, P. Zoller, Chiral quantum optics, Nature **541**, 473 (2017).

[18] C. Gonzalez-Ballestero, A. Gonzalez-Tudela, F. J. Garcia-Vidal, and E. Moreno, Chiral route to spontaneous entanglement generation, Phys. Rev. B **92**, 155304 (2015).

[19] K. Stannigel, P. Rabl, and P. Zoller, Driven-dissipative preparation of entangled states in cascaded quantum-optical networks, New J. Phys. **14**, 063014 (2012).

[20] T. Ramos, H. Pichler, A. J. Daley, and P. Zoller, Quantum Spin Dimers from Chiral Dissipation in Cold-Atom Chains, Phys. Rev. Lett. **113**, 237203 (2014).

[21] H. Pichler, T. Ramos, A. J. Daley, and P. Zoller, Quantum optics of chiral spin networks, Phys. Rev. A **91**, 042116 (2015).

[22] S. Mahmoodian, P. Lodahl, and A. S. Sørensen, Quantum Networks with Chiral Light Matter Interaction in Waveguides, Phys. Rev. Lett. **117**, 240501 (2016).

[23] C. Sayrin, C. Junge, R. Mitsch, B. Albrecht, D. O'Shea, P. Schneeweiss, J. Volz, and A. Rauschenbeutel, Nanophotonic Optical Isolator Controlled by the Internal State of Cold Atoms, Phys. Rev. X **5**, 041036 (2015).

[24] I. M. Mirza and J. C. Schotlan, Two-photon entanglement in multiqubit bidirectional-waveguide QED, Phys. Rev. A **94**, 012309 (2016).

[25] S. Raghu and F. D. M. Haldane, Analogs of quantum-Hall-effect edge states in photonic crystals, Phys. Rev. A **78**, 033834 (2008).

[26] M. C. Rechtsman, J. M. Zeuner, Y. Plotnik, Y. Lumer, D. Podolsky, F. Dreisow, S. Nolte, M. Segev, and A. Szameit, Photonic Floquet topological insulators, Nature (London) **496**, 196 (2013).

[27] L. Lu, J. D. Joannopoulos, and M. Soljačić, Topological photonics, Nat. Photonics **8**, 821 (2014).
[28] A. B. Khanikaev, S. Hossein Mousavi, W-K Tse, M. Kargarian, A. H. MacDonald, and G. Shvets, Photonic topological insulators, Nat. Mater. **12**, 233 (2013).
[29] Z. Wang, Y. D. Chong, J. D. Joannopoulos, and M. Soljačić, Reflection-Free One-Way Edge Modes in a Gyromagnetic Photonic Crystal, Phys. Rev. Lett. **100**, 013905 (2008).
[30] Z. Yu, G. Veronis, Z. Wang, and S. Fan, One-Way Electromagnetic Waveguide Formed at the Interface Between a Plasmonic Metal Under a Static Magnetic Field and a Photonic Crystal, Phys. Rev. Lett. **100**, 023902 (2008).
[31] Z. Wang, Y. Chong, J. D. Joannopoulos, and M. Soljačić, Observation of unidirectional backscattering immune topological electromagnetic states, Nature (London) **461**, 772 (2009).
[32] M. C. Rechtsman, Y. Plotnik, J. M. Zeuner, D. Song, Z. Chen, A. Szameit, and M. Segev, Topological Creation and Destruction of Edge States in Photonic Graphene, Phys. Rev. Lett. **111**, 103901 (2013).
[33] A. R. Davoyan and N. Engheta, Theory of Wave Propagation in Magnetized Near-Zero-Epsilon Metamaterials: Evidence for One-Way Photonic States and Magnetically Switched Transparency and Opacity, Phys. Rev. Lett. **111**, 257401 (2013).
[34] M. G. Silveirinha, Chern invariants for continuous media, Phys. Rev. B **92**, 125153 (2015).
[35] S. A. Hassani Gangaraj, A. Nemilentsau, and G. W. Hanson, The effects of three-dimensional defects on one-way surface plasmon propagation for photonic topological insulators comprised of continuum media, Sci. Rep. **6**, 30055 (2016).
[36] S. A. Hassani Gangaraj and G. W. Hanson, Topologically protected unidirectional surface states in biased ferrites: duality and application to directional couplers, IEEE Antennas Wireless Propag. Lett. **16**, 449 (2016).
[37] T. Gruner and D.-G. Welsch, Green-function approach to the radiation-field quantization for homogeneous and inhomogeneous Kramers-Kronig dielectrics, Phys. Rev. A **53**, 1818 (1996).
[38] H. T. Dung, L. Knöll, and D.-G. Welsch, Three-dimensional quantization of the electromagnetic field in dispersive and absorbing inhomogeneous dielectrics, Phys. Rev. A **57**, 3931 (1998).
[39] H. T. Dung, L. Knöll, and D.-G. Welsch, Spontaneous decay in the presence of dispersing and absorbing bodies: general theory and application to a spherical cavity, Phys. Rev. A **62**, 053804 (2000).
[40] S. Y. Buhmann, D. T. Butcher, and S. Scheel, Macroscopic quantum electrodynamics in nonlocal and nonreciprocal media, New J. Phys. **14**, 083034 (2012).
[41] G. Angelatos and S. Hughes, Entanglement dynamics and Mollow nonuplets between two coupled quantum dots in a nanowire photonic-crystal system, Phys. Rev. A **91**, 051803(R) (2015).
[42] Z. Ficek and R. Tanas, Entangled states and collective nonclassical effects in two-atom systems, Phys. Rep. **372**, 369 (2002).
[43] D. Martin-Cano, A. Gonzalez-Tudela, L. Martin-Moreno, F. J. Garcia-Vidal, C. Tejedor, and E. Moreno, Dissipation-driven generation of two-qubit entanglement mediated by plasmonic waveguides, Phys. Rev. B **84**, 235306 (2011).
[44] W. K. Wootters, Entanglement of formation and concurrence, Quantum Inf. Comput. **1**, 27 (2001).
[45] S. Ali Hassani Gangaraj, A. Nemilentsau, G. W. Hanson, and S. Hughes, Transient and steady-state entanglement mediated by three-dimensional plasmonic waveguides, Optics Express **23**, 22330 (2015).
[46] COMSOL Multiphysics ver. 5.2, COMSOL AB, Stockholm, Sweden, http://www.comsol.com.
[47] H-P Breuer and F. Petruccione, *The Theory of Open Quantum Systems* (Oxford University Press, New York, 2007).
[48] J. S. Bagby and D. P. Nyquist, Dyadic Greens functions for integrated electronic and optical circuits, IEEE Trans. Microwave Theory Tech. **35**, 207 (1987).
[49] A. Lakhtakia and T. G. Mackay, Vector spherical wavefunctions for orthorhombic dielectric-magnetic material with gyrotropic-like magnetoelectric properties, J. Opt. **41**, 201 (2012).
[50] M. G. Silveirinha, Bulk edge correspondence for topological photonic continua, Phys. Rev. B **94**, 205105 (2016).
[51] S. R. Seshadri, Excitation of surface waves on a perfectly conducting screen covered with anisotropic plasma, IRE Trans. Microwave Theory Tech. **10**, 573 (1962).